

# Phase Measurements of Barrier Crossings in a Periodically Modulated Double-Well Potential

Yeonee Seol<sup>1</sup>, D.L. Stein<sup>2</sup>, and Koen Visscher<sup>3</sup>

<sup>1</sup>*NHLBI, National Institute of Health, Bethesda, Maryland*

<sup>2</sup>*Departments of Physics and Mathematics, New York University and*

<sup>3</sup>*Department of Physics, University of Arizona*

(Dated: June 28, 2009)

## Abstract

We report on the experimental observation of the phase angle of a particle escaping over a periodically modulated potential barrier. Optical tweezers and back-focal plane position detection were used to record particle trajectories in the entire double-well potential. These measurements provide a sensitive test of theories proposed in the last decade of escape driven by random thermal noise from a periodically modulated potential. The observed phase shifts as a function of modulation frequency are consistent with those calculated using existing theories.

PACS numbers: 05.40.-a, 82.20.Uv

Investigations of thermally excited escape processes have a long history in theoretical physics, with the first modern, quantitative treatment provided by Kramers in 1940 [1] (for extensive reviews, see Hänggi et al. [2], Pollak and Talkner [3], and Reimann [4]). When the confining potential is time-dependent the barrier-crossing problem becomes more difficult to analyze, but its applicability also becomes more general. The case of periodically modulated forces in particular occurs in a number of physical contexts, such as stochastic resonance [5] and Brownian ratchets [6, 7]. It has consequently received significant theoretical [8–15] and increasing experimental attention [16–19].

Typically the escape rate is computed and measured as an average over the escape phase [10]. Here, we examine this problem at a more sensitive level, by quantitatively studying, both theoretically and experimentally, the phase angle between the barrier crossing event and the periodically modulated potential. A direct comparison between the two has so far been lacking.

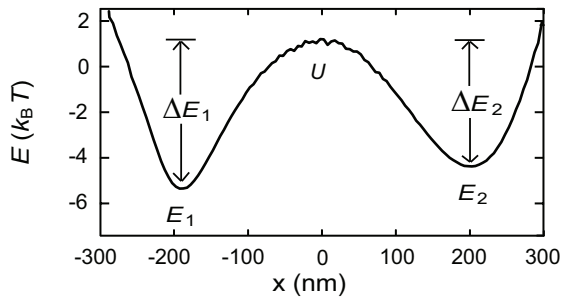


FIG. 1: Double-well potential as calculated from the position histogram of the polystyrene particle. Wells are indicated by  $E_1$  at  $x_1 \sim -188$  nm and  $E_2$  at  $x_2 \sim +200$  nm, while the barrier top  $U$  is located at  $x \sim +2$  nm. Barrier heights  $\Delta E_1$  and  $\Delta E_2$  are  $5.57 \pm 0.07 k_B T$  and  $4.79 \pm 0.02 k_B T$ , respectively.

*Experimental setup.* We generated an energy barrier separating two potential wells by positioning two time-shared optical traps in close proximity [17, 20], with the detailed structure of this double-well potential controlled by adjustment of the laser power and trap separation. A modified back-focal plane detection scheme enabled recording the trajectory of a trapped polystyrene particle (radius =  $0.325 \pm 0.005 \mu\text{m}$ ) in the full double-well potential (see suppl. info.). The supplemental information shows a representative time series of the particle’s x-position, enabling us to compute the one-dimensional trapping potential  $V(x)$  using the Boltzmann distribution  $P(x) = \exp(-V(x)/k_B T)$ , with  $P(x)$  the particle’s position his-

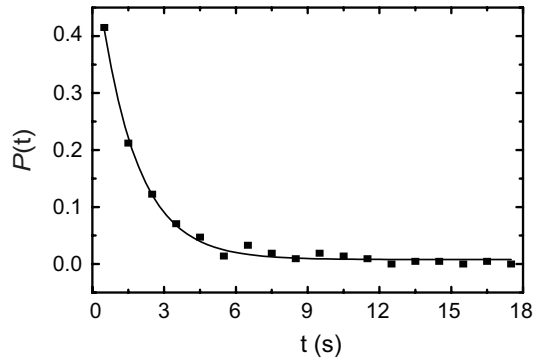


FIG. 2: Probability distribution of escape from well  $E_2$  in the absence of modulated force. The solid line (—) represents a fit of the data to a single-exponential decay function yielding a mean residence time of  $\tilde{\tau}_K = 1.6 \pm 0.1$  s ( $N = 364$  escapes).

togram. The potential is well-defined near the minima, but fluctuates significantly near the barrier where the particle spends relatively little time (Fig. 1). Detailed knowledge of  $V(x)$  then allows for a computation of the Kramers time  $\tau_K$  for each well. The barrier heights  $\Delta E_1$  and  $\Delta E_2$  are readily derived from  $V(x)$  (cf. Fig 1), whereas the local curvatures at the potential’s minima ( $k_{b_{1,2}}$ ) and barrier  $k_u$  follow from locally fitting to a quadratic. Within each well the potential fits to a quartic:  $V(x) \approx -(1/2)\mu^2 x^2 + (1/4)\lambda x^4$ , where  $\mu^2$  and  $\lambda$  are obtained from the local curvatures  $k$ , summarized in Table 1. The Kramers time  $\tau_K$  for each of the wells is given by Kramers’ equation  $\tau_{K_i} \cong \tau_{r_i} \exp(\Delta E_i/k_B T)$  with  $\tau_{r_i} = 2\pi\alpha/\sqrt{k_{b_i}k_u}$ , where  $\alpha = 6\pi r\eta$  is the viscous drag coefficient,  $r$  the radius of the particle, and  $\eta$  the medium viscosity (water). The particle center was  $\sim 800$  nm above the surface of the flow cell, requiring a correction to the viscous drag to account for the presence of the wall [21]. The Kramers times thus computed compares very well with the mean residence times directly determined from experimentally obtained time series of the particle’s position ( $\tilde{\tau}_K$ , Fig. 2 and Table 1). Such consistency provides confidence that our one-dimensional treatment of the activation process is reasonable [20].

Once the potential had been fully characterized, a periodic external field was added in order to create a modulated potential (periodic force) according to

$$\alpha\dot{x} = -V'(x) + A \cos(2\pi t/\tau_m) + \sqrt{2\alpha k_B T}\xi(t) \quad (1)$$

with  $x$  the system coordinate,  $V(x)$  the potential,  $\xi(t)$  a white noise,  $A$  the amplitude of the modulating force, and  $\tau_m$  its period. In practice, the periodic force was generated by

TABLE I: Numerical values for parameters of the potential well shown in Fig. 1, and characteristic time constants.

	$\Delta E$ ( $k_B T$ )	$ k $ (fN/nm)	$\tau_r$ (ms)	$\tau_K$ (s)	$\tilde{\tau}_K$ (s)
$E_1$	$5.57 \pm 0.07$	$8.9 \pm 0.3$	$7.7 \pm 0.2$	$2.4 \pm 0.1$	$2.3 \pm 0.2$
$E_2$	$4.79 \pm 0.02$	$4.4 \pm 0.1$	$11.0 \pm 0.2$	$1.5 \pm 0.2$	$1.6 \pm 0.1$
U	-	$1.60 \pm 0.01$	-	-	-

changing the laser intensities of the two traps with identical amplitude but with opposite phase. Note that we only investigate the transitions from one trap over the barrier, so that the phase relation between the two traps is irrelevant to our results. In practice, the opposite phase relation proved helpful in restoring the particle to the trap of interest. The force amplitude,  $A$ , was then computed as the slope of potential well difference between the potential shown in Fig. 1 and the potential with a higher laser intensity. Because of the significant uncertainty in both potentials in the vicinity of the barrier, the force magnitude can be estimated only to within a factor of two:  $A \sim 15 - 30$  fN.

*Phase shifts.* While previous experiments have characterized escape dynamics in terms of residence time distributions [16, 20], we focused on determining the phase angle and its dependence upon the frequency of the external modulation. A modulation reference signal was obtained by low-pass filtering the AOD driving signal while accounting for any undesired phase shifts incurred upon filtering. The modulation reference signal and particle position were recorded simultaneously, enabling computation of the phase angle. The experimental escape phase, or phase angle, was defined as indicated in Fig. 3: it is the time from the nearest previous maximum in the modulation reference signal to the barrier crossing event.

A phase angle of  $\pi$  is assigned when the crossing occurs with the barrier at its minimal height (at time  $\tau_m/2$ ). We have determined the phase angle for transitions from potential  $E_2$  into  $E_1$ . Three time constants are of importance in this dynamical system:  $\tau_r$ , the Kramers prefactor;  $\tau_K$ , the Kramers time; and  $\tau_m$ , the modulation period of the external driving field. Modulation periods  $\tau_m$  ranged from much smaller than, up to the order of, the Kramers time, i.e., from 62.5 ms to 1 s. Experimental results are presented in Fig. 4 (solid squares), where we show the transition probability versus the phase angle.

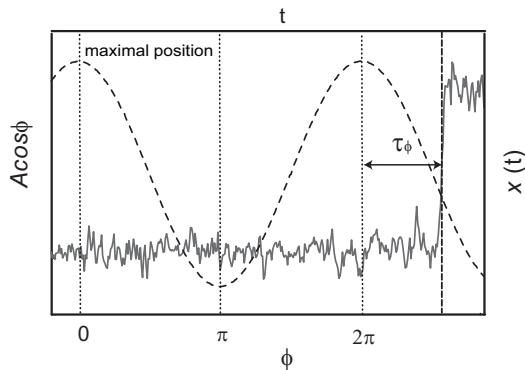


FIG. 3: Definition of the escape phase angle,  $\tau_\phi$ , expressed as a fraction of the modulation period  $\tau_m$ .  $\tau_\phi$  equals the time from the point where the particle passes the potential barrier top to the nearest previous maximum of the phase signal.

As noted, a phase angle of  $\pi$  (corresponding to a time  $\tau_m/2$ ) corresponds to a barrier minimum, and not surprisingly, the transition probabilities tend to peak around this point. However, at modulation times close to the Kramers time ( $\tau_m = 1$  s and  $\tau_K = 1.5$  s), the probability maximum has shifted towards the left, i.e., towards smaller phase angles. We interpret this shift as follows: as  $\tau_m$  increases, the escape dynamics are determined increasingly by the mechanisms leading to the ordinary Kramers time in the static case; consequently, escape may occur well before the barrier has reached a minimum. In the limit  $\tau_m \rightarrow \infty$  one expects to recover standard Kramers decay, as in Fig. 2. However, at shorter modulation times, for example 62.5 ms and 250 ms with  $\tau_r \ll \tau_m \ll \tau_K$ , we expect transitions to occur when the barrier is near a minimum: in this regime the driving force dominates the escape dynamics. These arguments capture the essential qualitative trends seen in the data; however, a detailed theoretical analysis is required to uncover the intricacies of the dynamics involved and to quantitatively predict the observed phase angles. We discuss this in the next section.

*Theoretical analysis.* Previous treatments [8–13, 16] can be used to analyze escape rates in the experimental setup described above. Because all are in fundamental agreement, we use the approach of [10], to which we refer the reader for details.

The unperturbed (static) potential  $V(x)$  was quartic:  $V(x) = (-1/2)\mu^2 x^2 + (1/4)\lambda x^4$ , with  $\mu^2 = 1.9$  fN/nm and  $\lambda = 4.64 \times 10^{-5}$  fN/nm<sup>3</sup>; this was then subjected to a periodic forcing amplitude of magnitude  $A \simeq 15 - 30$  fN. The analysis depends on the relative

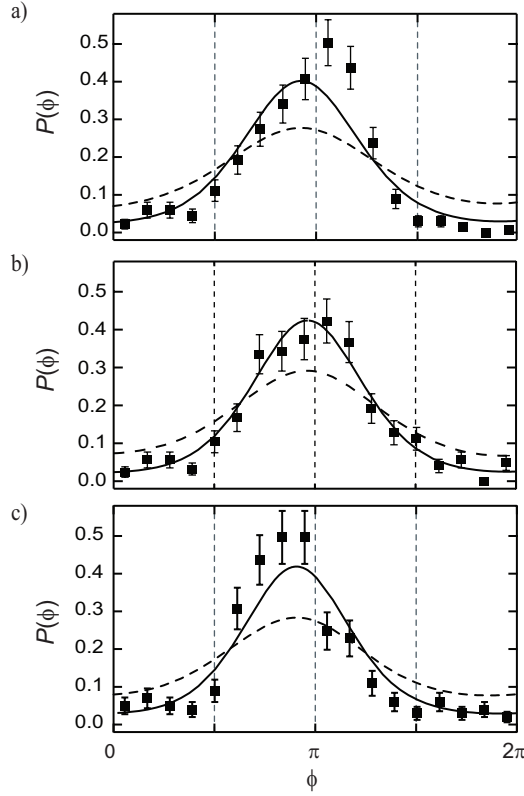


FIG. 4: Experimental and theoretical escape probabilities vs. phase angle. a)  $\tau_m = 62.5$  ms; b)  $\tau_m = 250$  ms; c)  $\tau_m = 1$  s. Solid squares: experimental data; dashed and solid lines: escape probabilities  $P(\phi)$  (Eq. (4)) with force amplitudes of  $A = 15$  fN, and  $A = 30$  fN, respectively.

magnitudes of  $A$  and  $\sqrt{2m\omega_u^2 k_B T}$ , where  $\omega_u = \sqrt{U''(x_u)/m}$  is the oscillation frequency about  $x_u$ , the top of the well. We find that  $\sqrt{2m\omega_u^2 k_B T} \approx 0.4$  pN, roughly a factor of 15-30 larger than  $A$ , indicating that a perturbative modification of Kramers' theory can be used [10].

Let  $x_*(t)$  denote an optimal escape trajectory when  $A = 0$  (see [22] for how these are determined), and consider the family  $x_*^{(\phi)}(t) \equiv x_*(t - \frac{\phi}{2\pi}\tau_m)$  of phase-shifted trajectories, where the phase angle  $\phi$  satisfies  $0 \leq \phi < 2\pi$ . Then the first-order (in  $A$ ) correction to the unperturbed energy barrier  $\Delta E$  will be  $Aw_1(\phi)$ , where  $w_1(\phi) = -\int_{-\infty}^{\infty} \dot{x}_*^{(\phi)}(t)\nu(t) dt$ . For the quartic potential, we then find for the instantaneous phase-dependent escape rate  $\lambda(\phi)$ ,

$$\lambda(\phi) \sim \tau_K^{-1} \exp\left[-\frac{A\mu^3}{2k_B T \alpha \sqrt{\lambda}} \int_{-\infty}^{\infty} dt f(t)\right] \quad (2)$$

$$f(t) = \frac{\exp[-\frac{\mu^2}{\alpha}(t - \omega_m \phi)]}{\left(1 + \exp[-\frac{\mu^2}{\alpha}(t - \omega_m \phi)]\right)^{3/2}} \cos(\omega_m t). \quad (3)$$

Although the “phase shift” approach of [10] employs a different analysis from other investigations of this problem, most notably the “logarithmic susceptibility” approach of [8], both arrive at the expression above for the phase-dependent escape rate.

The phase-dependent escape rates  $\lambda(\phi)$  are shown in Fig. 5 using the experimental numbers given above for the 3 different modulation times:  $\tau_m = 62.5$  ms, 250 ms, and 1 s. It is interesting to note that the phase angle maxima of  $\lambda(\phi)$  slightly *decreases* as  $\tau_m$  decreases, contrary to experimental observation. However,  $\lambda(\phi)$  is not the quantity measured; rather, the correct stochastic quantity to compare to is the phase angle when the particle *first* escapes its confining well. We will denote by  $\mathcal{P}(\phi)$  the probability that a particle escapes when the system is at phase angle  $\phi$ , conditioned on its *not* having escaped prior to that time. If  $\phi_0$  is the system’s phase angle when a particular run begins, and  $P(\phi_0)$  is its probability density over many runs, then  $\mathcal{P}(\phi)$  is given by  $\mathcal{P}(\phi) = \sum_{n=0}^{\infty} P(\phi_0 + 2\pi n)$  with  $0 \leq \phi < 2\pi$  and

$$P(\phi) = \frac{\lambda(\phi)}{2\pi\omega_m} \int_0^{2\pi} d\phi_0 P(\phi_0) \exp \left[ - \int_0^{(\phi-\phi_0)/\omega_m} d\phi' \lambda(\phi') \right], \quad (4)$$

with  $\phi_0 \leq \phi < \infty$  in (4).

Fig. 4 (solid and dashed lines) shows  $\mathcal{P}(\phi)$ , which displays the qualitative (and quantitative, for  $A = 30$  fN) behavior observed in experiment. In particular, the shift of the probability maximum towards smaller phase angle for longer modulation times is predicted and agrees both qualitatively and quantitatively with the experimentally determined shift.

*Discussion.* Because the experiment permits us to determine the modulation force amplitude  $A$  only to within a factor of two, we show in Fig. 4 two fits, with the force at either end of the range: one with  $A = 15$  fN and the other with  $A = 30$  fN. We see that the better fit occurs with the larger force, and that the theory agrees with the experiment within experimental uncertainty.

Future experiments can improve this test of the theory in at least two ways. It is clear that a more accurate determination of the modulating force is necessary for further progress. This is experimentally challenging, however, as it requires a sensitive determination of the static and perturbing potentials near the barrier. The obvious difficulty in doing this arises from the particle’s spending comparatively little time in this region. Therefore, either a method other than using time series needs to be developed, or else a significant increase in the number of escape trajectories is required.

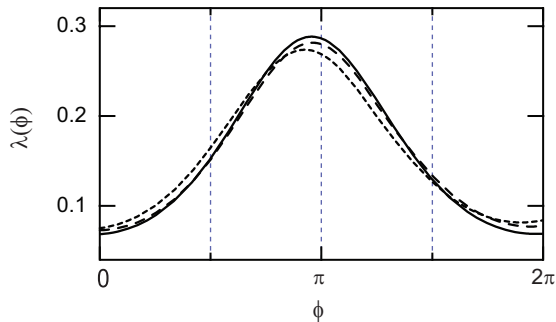


FIG. 5: Phase-dependent escape rates,  $\lambda(\phi)$ , at  $\tau_m = 62.5$  ms (short dash);  $\tau_m = 250$  ms (long dash);  $\tau_m = 1$  s (solid).

A second intriguing feature is the suggestion in the data (cf. Fig. 4) of a developing asymmetry in the escape probability vs. phase angle as the modulation time becomes shorter (62.5 ms). The theoretical curves do not appear to reflect this behavior. However, given the increasing roughness of the data, particularly as one moves away from the probability maximum, it is difficult to ascertain whether such an effect is actually present. If in fact this asymmetry is real, our theory may fail to capture it because it always assumes that the experiment is in the adiabatic regime, i.e., that  $\tau_r \ll \tau_m$ , whereas  $\tau_r \approx 0.2\tau_m$  when  $\tau_m = 62.5$  ms. Further theoretical and experimental explorations in the very short-time regime will be required to resolve this issue. Another possibility arises from an interesting observation made in [23], where non-conservative forces due to radiation pressure may potentially give rise to three-dimensional circulation of particles, which could affect escape kinetics. Even though this observation has recently been contested [24], the particle used in that paper was roughly a factor of 3-4 larger, which gives rise to much higher forces due to radiation pressure than in our case. We would further expect that the agreement we observed between the calculated and measured Kramers times ( $\tau_K$  and  $\tilde{\tau}_K$ ) would not have occurred if such three-dimensional motion had been important, so we suspect that this effect, if present, plays no role in our experiment. It is also interesting to note that an asymmetry was predicted in Dykman and Rykvine [13] (cf. Fig. 2) for the instantaneous escape rate. This is owing to two factors playing against each other: the modulation frequency times the relaxation time at the top of the barrier vs. the ratio of the strength of the modulating force to the noise intensity. In our experiment, the first of these is no larger than 0.2 at the shortest modulation times, while the latter is roughly  $10^{-2}$ . Because the asymmetry occurs when at

least one of these two factors is large, this is unlikely to be the cause of the asymmetry in our experiment. It would be of great interest to determine in future experiments whether such an asymmetry really exists in the experimental regime considered here.

Summarizing, we have experimentally verified theoretical predictions of the phase angle of escape for a particle subject to a modulating force and weak external noise. We note that the large bandwidth of the detection system used here should be particularly beneficial for studying underdamped systems where the slowly damped oscillations may be quite fast.

*Acknowledgments.* We thank Robert Maier for extensive discussions when the experiment was being performed, and Mark Dykman for helpful comments on the paper. DLS was supported in part by NSF Grants PHY-0351964, PHY-0601179, and PHY-0651077. While at the University of Arizona YS was supported in part by NSF PHY-0099484.

- 
- [1] H. A. Kramers, *Physica* **7**, 284 (1940).
  - [2] P. Hänggi et. al *Rev. Mod. Phys.* **62**, 251 (1990).
  - [3] E. Pollak, and P. Talkner, *Chaos* **15**, 026116 (2005).
  - [4] P. Reimann, *Phys. Repts.* **361**, 57 (2002).
  - [5] L. Gammaitoni, et al. *Rev. Mod. Phys.* **70**, 223 (1998).
  - [6] M. O. Magnasco, *Phys. Rev. Lett.* **71**, 1477 (1993).
  - [7] Ya. M. Blanter and M. Büttiker, *Phys. Rev. Lett.* **81**, 4040 (1998).
  - [8] V. N. Smelyanskiy, et. al *Phys. Rev. Lett.* **82**, 3193 (1999).
  - [9] J. Lehmann, et. al *Phys. Rev. Lett.* **84**, 1639 (2000).
  - [10] R. S. Maier and D. L. Stein, *Phys. Rev. Lett.* **86**, 3942 (2001).
  - [11] N. Berglund and B. Gentz, *J. Diff. Eq.* **191**, 1 (2003).
  - [12] M. I. Dykman and D. Rykvine, *Phys. Rev. Lett.* **94**, 070602 (2005).
  - [13] M. I. Dykman and D. Rykvine, *Phys. Rev. E* **72**, 011110 (2005).
  - [14] H.-J. Lin, et. al, *Phys. Rev. Lett.* **98**, 088304 (2007).
  - [15] H.-J. Lin, et. al, *J. Chem. Phys.* **128**, 084708 (2008).
  - [16] M. I. Dykman, et. al, *Chaos* **11**, 587 (2001).
  - [17] A. Simon and A. Libchaber, *Phys. Rev. Lett.* **68**, 3375 (1992).
  - [18] P. Jop, et. al, *Europhys. Lett.* **81**, 50005 (2008).

- [19] O. Braun, et. al, *Phys. Rev. Lett.* **93**, 158105 (2004).
- [20] L. I. McCann, et. al, *Nature* **402**, 785 (1999).
- [21] K.C. Neuman and S.M. Block, *Rev. Sci. Instr.* **75**, 2787 (2004) .
- [22] R. S. Maier and D. L. Stein, *Phys. Rev. E* **48**, 931 (1993).
- [23] Y. Roichman, et. al, *Phys. Rev. Lett.* **101**, 128301 (2008).
- [24] R. Huang, P. Wu, and E.-L. Florin, [arxiv.org/0806.4632](https://arxiv.org/abs/0806.4632).